


EARTH SCIENCES

Partial offset of soil greenhouse gases emissions by enhanced vegetation carbon uptake upon thermokarst formation

Zhihu Zheng^{1,2,3}, Chunbao Zhao^{1,2,3}, Guibiao Yang^{1,2}, Wei Zhou^{1,2,3}, Bin Wei^{1,2,3}, Yuhong Xie^{1,2,3}, Yunfeng Peng^{1,2}, Leiye Chen^{1,2}  and Yuanhe Yang^{1,2,3,*}

Permafrost-affected regions contain 1014 Pg (1 Pg = 10^{15} g) carbon (C) and 67 Pg nitrogen (N) in the top 3 meters of the soil profile [1,2]. Over the past few decades, sustained climate warming has triggered widespread permafrost thaw, manifested primarily through active layer thickening and thermokarst landscape formation [3]. Extensive thawing of the permafrost exposes previously frozen organic matter to microbial decomposition, releasing greenhouse gases (GHGs) in the form of carbon dioxide (CO₂), methane (CH₄), and nitrous oxide (N₂O). As potent climate forcers, these GHG emissions can amplify climate warming, driving a strong positive permafrost C- and N-climate feedback loop [2,4]. Compared to gradual active layer thickening, thermokarst formation induces abrupt reorganization of hydrological regimes, vegetation patterns, and soil processes over landscape scale, thereby exerting more pronounced influences on regional C and N cycles [2,4–7]. Therefore, elucidating impacts of thermokarst formation on GHG fluxes is critical for accurately assessing the strength of permafrost C- and N-climate feedbacks.

Recent decades have witnessed substantial advances in how thermokarst formation influences GHG fluxes and their driving forces [8–11]. It has been reported that thermokarst formation accelerates soil respiration [11], particularly through mobilizing old permafrost C [8], and also triggers non-CO₂ feedback via increasing CH₄ and N₂O

emissions [2,6]. Although prior studies have advanced our understanding on this research field, there remain two critical conceptual and mechanistic gaps. First, previous studies focused on the GHG emission process, with vegetation-mediated CO₂ uptake being largely overlooked. This scenario obscured whether post-thaw nutrient mobilization [12] could mediate vegetation growth and counteract soil GHG emissions, thereby creating systematic biases in the net ecosystem C budget. Second, previous studies mainly attributed thaw-induced changes in GHG fluxes to abiotic factors (e.g. soil temperature and moisture) [9,10], with the potential role of biotic drivers (e.g. plant functional traits and microbial functional genes) in mediating GHG trajectories being largely unexplored. Therefore, quantifying ecosystem-scale GHG budgets by integrating vegetation C sequestration and decoding the biological mechanisms mediating these fluxes, represent urgent priorities for better predicting the permafrost-climate feedback.

The Tibetan Plateau, the largest high-altitude permafrost region in the Northern Hemisphere, is undergoing rapid climate warming coupled with proliferating thermokarst landscapes, providing an ideal platform for addressing the above knowledge gaps. To this end, we established a regional-scale thermokarst monitoring network across the Tibetan alpine permafrost region. Through standardized *in-situ* observations, we determined the

changes in three GHG emissions upon thermokarst formation and quantified the contribution of vegetation-mediated CO₂ uptake to the net ecosystem GHG budget. Additionally, we deciphered biological mechanisms underlying GHG flux responses via plant functional traits and microbial functional genes. Specifically, we identified five representative thermo-erosion gullies across typical permafrost regions (i.e. Madoi and Qilian Mountain; Fig. S1a). In each gully, triplicate sampling plots were established separately in the non-collapsed areas, early and late stages of permafrost thaw (Fig. S1b–i). Using a CH₄/CO₂ infrared gas analyzer and LI-7820 soil N₂O/H₂O flux measurement system, we measured GHG emissions (including ecosystem respiration [ER], CH₄, and N₂O fluxes) as well as vegetation C uptake (gross primary productivity [GPP]). This study aims to address the following three key questions: (1) how do CO₂, CH₄, and N₂O fluxes change along the thaw sequence? (2) How does thermokarst formation influence the extent of plant C uptake offsetting GHG emissions? (3) What are the biological mechanisms that underlie GHG flux in response to thermokarst formation?

Based on two years of field measurements, we examined the responses of GHG fluxes to thermokarst formation using linear mixed-effects models, where thaw stage was set as the fixed effect and thermokarst-impacted site was treated as a random effect, the other variables are

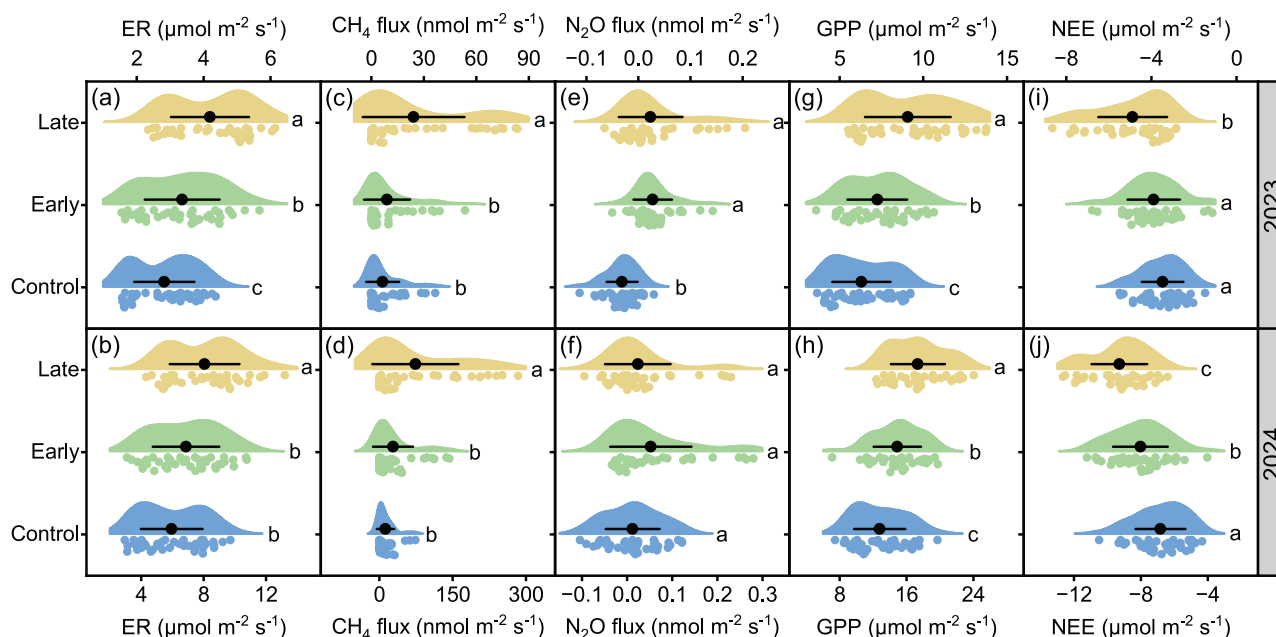


Figure 1. Changes in ecosystem respiration (ER; a, b), CH_4 fluxes (c, d), N_2O fluxes (e, f), gross primary productivity (GPP; g, h), and net ecosystem exchange (NEE; i, j) along the thaw sequence at the five thermokarst-affected sites during the growing seasons of 2023 and 2024. Dots of different colors represent the corresponding data from the control (blue), early (green), or late (yellow) thaw stage. Each dot below the violin represents an individual data point. Black dot within the violin shows the mean value, and the error bar denotes SD ($n = 40$). These comparisons were analysed based on linear mixed-effects models with one-sided F tests, where thaw stage was set as the fixed effect and thermokarst-impacted site was treated as a random effect. Significant differences are denoted by different letters among the different thaw stages ($P < 0.05$).

the same. Our results revealed consistent GHG responses to thermokarst formation between the two experimental years. Specifically, permafrost collapse accelerated microbial mineralization and led to a 15.4%–48.6% increase in ER (Fig. 1a and b). This trend aligns with substantial soil organic C depletion (Fig. S2a), highlighting the accelerated release of stored C following permafrost thaw. In addition to ER, we found a pronounced intensification of CH_4 emission under thermokarst progression. To be specific, early-stage emissions remained statistically indistinct from non-collapsed areas, whereas late-stage fluxes increased by 277.0%–498.8% during the two observational years (Fig. 1c and d). The increase in CH_4 fluxes may be attributed to changes in soil water-filled pore space (WFPS) [7]. Permafrost collapse typically compacts soils and reduces porosity, resulting in an increased WFPS (Fig. S2b). Such hydrological reconfiguration would exacerbate soil anaerobic conditions, thereby favoring growth of methanogenesis. To further decipher microbial drivers of

these fluxes, we quantified the abundance of functional genes involved in the CH_4 cycle using qPCR. Our results revealed divergent responses between key microbial functional genes: the abundance of *mcrA* genes (marker for methanogens) significantly increased, while the *pmoA* genes (marker for methanotrophs) showed marked reduction after permafrost collapse (Fig. S4a and b). These findings demonstrate that thermokarst formation creates a more anaerobic environment at the late thaw stage, thereby shifting microbial communities toward methanogen dominance while suppressing methanotrophic oxidation. These microbial community changes ultimately drove an enhancement of CH_4 emission at the late thaw stage.

Besides C emissions, we explored the impacts of thermokarst formation on N_2O flux. Our results demonstrated that the formation of thermokarst landforms enhanced N_2O emissions (Fig. 1e and f). Notably, exposed patches exhibited exceptionally high emission rates (1.37 vs 0.01 $\text{nmol m}^{-2} \text{s}^{-1}$), surpassing

both non-collapsed areas and vegetated patches within collapsed zones (Fig. S5), reaching levels comparable to high-emission ecosystems such as tropical forests and croplands [2]. We further found that the increased availability of substrates and functional microbial gene abundance were responsible for the thermokarst-induced rise in N_2O emissions. On the one hand, soil NO_3^- -N content is a primary driver of N_2O flux variations. Particularly, when WFPS exceeds the 65% threshold, denitrification dominates N_2O production [2]. Thermokarst formation facilitated the release of previously frozen NO_3^- -N from permafrost, thereby elevating soil NO_3^- -N availability. This phenomenon was particularly pronounced in exposed patches, where the absence of plant N uptake resulted in significantly higher NO_3^- -N content (Figs S2d–f and S6). The enrichment of this key denitrification substrate consequently stimulates N_2O emissions. On the other hand, functional microbes are recognized as critical drivers of N_2O dynamics [2].

Analysis of nitrification-associated microbial genes revealed significant increases in ammonia-oxidizing bacteria (AOB) gene abundance in both vegetated and exposed patches after permafrost collapse, while ammonia-oxidizing archaea (AOA) gene abundance remained unchanged (Figs S4c, d and Fig. S7). Further analysis of denitrification-related genes (*nirK* and *nirS*, encoding nitrite reductase; *nosZ*, encoding N_2O reductase) demonstrated a greater ($(\text{nirK} + \text{nirS})/\text{nosZ}$) ratio in exposed patches but remained stable in vegetated patches after permafrost collapse (Figs S4e–h and S8). These microbial community shifts indicate the concurrent intensification of nitrification and denitrification processes upon thermokarst formation, driving an escalation of N_2O emission.

Despite the increment of GHG emission, we found that GPP and net ecosystem exchange (NEE) increased by 15.1%–44.0% (Fig. 1g and h) and 11.9%–40.3% (Fig. 1i and j) upon thermokarst formation, respectively. These patterns aligned with concurrent increases in aboveground biomass (AGB), belowground biomass (BGB), and Normalized Difference Vegetation Index (NDVI) at the late thaw stage (Fig. S3), suggesting that thermokarst formation promotes vegetation growth and enhances vegetation C fixation. To identify the dominant drivers of GPP enhancement along the thaw sequence, we measured a number of influential factors along the thaw gradient. Our results showed that the increased plant P uptake was likely a key driver for the stimulation of GPP upon thermokarst formation, which was supported by our previous work [13], while other factors seem to have limited effects on GPP improvement (see Supplementary Note 1 for detailed discussion). This improvement of plant P uptake (as evidenced by leaf P enrichment) likely resulted from the post-thaw enhancements in soil gross phosphate (Pi) mobilization. In support of this deduction, a recent study from our research group revealed that thermokarst formation altered the relative abundances of those microbial genes involved in P-cycling processes and enhanced the soil

microbial capabilities for mineralization and solubilization of P. The enhanced abundances of P-cycling functional genes for organic P mineralization and inorganic P solubilization likely drove the accelerated gross Pi mobilization upon permafrost collapse, which could then stimulate plant P uptake and elevate foliar P content. Given the established linkages between foliar P content and plant photosynthetic efficiency [14], the trait-based changes may drive GPP enhancement in thermokarst-affected areas.

In summary, based on two growing seasons of field measurements, we systematically evaluated the impacts of thermokarst formation on ecosystem CO_2 , CH_4 , and N_2O fluxes. Our two consecutive years' observations consistently revealed that thermokarst formation tended to increase GHG emissions and also stimulated vegetation C fixation. We further calculated the combined radiative forcing through CO_2 equivalent conversion for GHG emissions (including ER, CH_4 , and N_2O fluxes) and vegetation C uptake (GPP). We found the GHG emissions increased by 35.3% (18.3%–55.6%), while vegetation C uptake increased by 27.8% (15.1%–44.0%) after thermokarst formation, suggesting that thermokarst-induced enhancement of plant C uptake partially offsets ecosystem GHG emissions. This finding emphasizes the importance of considering the contribution of vegetation when assessing future permafrost C- and N-climate feedbacks. Despite the advances made so far, our study still has two limitations: the relatively low-frequency of *in-situ* GHG flux observations and exclusive focus on growing-season dynamics. It has been reported that GHG pulse emissions during non-growing seasons, particularly shoulder seasons, account for ~24.1% of annual GHG emissions [15–17]. Meanwhile, winter GHG emissions are projected to exhibit a substantial increasing trajectory under future climate scenarios [18]. Future efforts should thus integrate year-round high-frequency monitoring to capture complete GHG budgets, enabling more precise prediction of the direction and magnitude of permafrost-

climate feedback under future climate scenarios.

SUPPLEMENTARY DATA

Supplementary data are available at [NSR](#) online.

ACKNOWLEDGMENTS

The authors would like to thank G.Q. Wang and E.T. Liu for their help with the establishment of the thermokarst monitoring network. The authors also appreciate three anonymous reviewers for their insightful comments on an early version of this paper.

FUNDING

This work was supported by the National Key Research and Development Program of China (2022YFF0801903) and the National Natural Science Foundation of China (32588202, 32425004 and 32201359).

AUTHOR CONTRIBUTIONS

Y.Y., Z.Z. and G.Y. designed this research. Z.Z., C.Z., W.Z., B.W. and Y.X. performed field samplings and measurements. Z.Z. performed laboratory experiments. Z.Z. analysed the data. Z.Z., G.Y., Y.P., L.C. and Y.Y. wrote the manuscript.

Conflict of interest statement. None declared.

Zhihu Zheng^{1,2,3}, Chunbao Zhao^{1,2,3},
Guibiao Yang^{1,2}, Wei Zhou^{1,2,3}, Bin Wei^{1,2,3},
Yuhong Xie^{1,2,3}, Yunfeng Peng^{1,2},
Leiyi Chen^{1,2} and Yuanhe Yang^{1,2,3,*}

¹State Key Laboratory of Forage

Breeding-by-Design and Utilization; Key Laboratory of Vegetation and Environmental Change, Institute of Botany, Chinese Academy of Sciences, China;

²China National Botanical Garden, China and

³College of Resources and Environment, University of Chinese Academy of Sciences, China

*Corresponding author.

E-mail: yhyang@ibcas.ac.cn

REFERENCES

- Mishra U, Hugelius G, Shelef E *et al.* *Sci Adv* 2021; **7**: eaaz5236.
- Voigt C, Marushchak ME, Abbott BW *et al.* *Nat Rev Earth Environ* 2020; **1**: 420–34.
- Olefeldt D, Goswami S, Grosse G *et al.* *Nat Commun* 2016; **7**: 13043.
- Turetsky MR, Abbott BW, Jones MC *et al.* *Nat Geosci* 2020; **13**: 138–43.

5. Miner KR, Turetsky MR, Malina E *et al.* *Nat Rev Earth Environ* 2022; **3**: 55–67.
6. Schuur EAG, Abbott BW, Commane R *et al.* *Annu Rev Environ Resour* 2022; **47**: 343–71.
7. Chen L, Yang G, Bai Y *et al.* *Sci China Life Sci* 2024; **67**: 1833–48.
8. Estop-Aragonés C, Olefeldt D, Abbott BW *et al.* *Glob Biogeochem Cycle* 2020; **34**: e2020GB006672.
9. Abbott BW and Jones JB. *Glob Change Biol* 2015; **21**: 4570–87.
10. Mu CC, Abbott BW, Zhao Q *et al.* *Geophys Res Lett* 2017; **44**: 8945–52.
11. Wang G, Peng Y, Chen L *et al.* *Nat Geosci* 2024; **17**: 532–8.
12. Finger RA, Turetsky MR, Kielland K *et al.* *J Ecol* 2016; **104**: 1542–54.
13. Yang G, Peng Y, Abbott BW *et al.* *Glob Change Biol* 2021; **27**: 5818–30.
14. Lombardozzi DL, Smith NG, Cheng SJ *et al.* *Environ Res Lett* 2018; **13**: 074025.
15. Li Q, Liu Y, Kou D *et al.* *Glob Change Biol* 2022; **28**: 5200–10.
16. Bao T, Xu X, Jia G *et al.* *Glob Change Biol* 2021; **27**: 376–87.
17. Wolf B, Zheng X, Brüggemann N *et al.* *Nature* 2010; **464**: 881–4.
18. Natali SM, Watts JD, Rogers BM *et al.* *Nat Clim Chang* 2019; **9**: 852–7.